Succinate dehydrogenase-deficiency in a chromaffin cell model retains metabolic fitness through the maintenance of mitochondrial NADH oxidoreductase function

Thakker, Alpesh

Published in:
Faseb Journal

Publication date:
2020

Received: 14 June 2019 | Revised: 17 September 2019 | Accepted: 8 October 2019

DOI: 10.1096/fj.201901456R

RESEARCH ARTICLE

THE FASEB JOURNAL

Succinate dehydrogenase deficiency in a chromaffin cell model retains metabolic fitness through the maintenance of mitochondrial NADH oxidoreductase function

Katarína Kľučková[1] | Alpesh Thakker[1] | Lisa Vettore[1] | Cristina Escribano-Gonzalez[1] | Rebecca L. Hindshaw[1] | Jacqueline L. E. Tearle[1] | Judith Goncalves[2] | Baksho Kaul[1] | Gareth G. Lavery[1] | Judith Favier[2] | Daniel A. Tennant[1]

[1]Institute of Metabolism and Systems Research, College of Medical and Dental Sciences, University of Birmingham, Birmingham, UK

[2]Université de Paris, PARCC, INSERM, Equipe Labellisée par la Ligue contre le Cancer, Paris, France

Correspondence
Judith Favier, PARCC, European Georges Pompidou Hospital, 56 rue Leblanc, 75015 Paris, France.
Email: judith.favier@inserm.fr

Daniel A. Tennant, Institute of Metabolism and Systems Research, College of Medical and Dental Sciences, University of Birmingham, Birmingham B15 2TT, UK.
Email: d.tennant@bham.ac.uk

Present address
Katarína Kľučková, Barts Cancer Institute, Queen Mary University of London, London, UK

Abstract

Mutations in succinate dehydrogenase (SDH) lead to the development of tumors in a restricted subset of cell types, including chromaffin cells and paraganglia. The molecular basis for this specificity is currently unknown. We show that loss of SDH activity in a chromaffin cell model does not perturb complex I function, retaining the ability to oxidize NADH within the electron transport chain. This activity supports continued oxidation of substrates within the tricarboxylic acid (TCA) cycle. However, due to the block in the TCA cycle at SDH, the high glutamine oxidation activity is only maintained through an efflux of succinate. We also show that although the mitochondria of SDH-deficient cells are less active per se, their higher mass per cell results in an overall respiratory rate that is comparable with wild-type cells. Finally, we observed that when their mitochondria are uncoupled, SDH-deficient cells are unable to preserve their viability, suggesting that the mitochondrial metabolic network is unable to compensate when exposed to additional stress. We therefore show that in contrast to models of SDH deficiency based on epithelial cells, a chromaffin cell model retains aspects of metabolic "health," which could form the basis of cell specificity of this rare tumor type.

Abbreviations: DTNB, 5,5′-dithiobis-(2-nitrobenzoic acid); ETC, electron transport chain; ETF, electron transfer flavoprotein; FA, fatty acids; FAO, fatty acid oxidation; FCCP, carbonyl cyanide 4-(trifluoromethoxy)phenylhydrazone; GIST, gastrointestinal stromal tumors; imCC, immortalized murine chromaffin cells; MAF, mouse adrenal fibroblasts; ME2, malic enzyme 2; NAD^+, nicotinamide adenine dinucleotide; NADH, reduced NAD^+; OAA, oxaloacetate; PCK2, phosphoenolpyruvate carboxykinase; PDH E1α, pyruvate dehydrogenase E1α subunit; PDK1/4, PDH kinase 1/4; PPGL, pheochromocytoma and paraganglioma; RIPA, radioimmunoprecipitation assay; ROS, reactive oxygen species; SDHA-D, succinate dehydrogenase subunits A-D; SRB, sulforhodamine B; TCA, tricarboxylic acid; TMRE, Tetramethylrhodamine ethyl ester; UCP2, uncoupling protein 2.

Jacqueline L. E. Tearle, EMBL Australia Single Molecule Science, School of Medical Sciences, Lowy Cancer Research Centre, UNSW, Sydney, Australia

Funding information
Paradifference; Wellcome Trust (Wellcome), Grant/Award Number: 104612/Z/14/Z; Cancer Research UK (CRUK), Grant/Award Number: C42109/A26982 and C42109/A24891

KEYWORDS
electron transport chain, metabolism, mitochondria, pheochromocytoma, succinate dehydrogenase

1 | INTRODUCTION

Succinate dehydrogenase (SDH), also known as complex II (CII) of the electron transport chain (ETC), has a unique function within the mitochondrial metabolic network, being part of both the ETC and the tricarboxylic acid (TCA) cycle. As such, SDH activity was thought to be universally required for cell proliferation and survival. However, loss of any one of the four subunits of this enzyme leads to the development of rare tumor types including pheochromocytoma and paraganglioma (PPGL), gastrointestinal stromal tumors (GIST), and cases of renal cancer.[1] The function of SDH within the mitochondrial matrix is to oxidize succinate to fumarate with the resulting electrons reducing the ubiquinone pool of the ETC. SDH deficiency therefore results in a well-characterized increase in succinate levels in the matrix, which on reaching the cytosol inhibits members of the 2-oxoglutarate-dependent dioxygenase family of enzymes, eliciting epigenetic changes and pseudohypoxic signaling that are likely the major drivers of tumorigenesis.[2,3]

However, despite being originally described in 2000,[4] little is still known concerning how loss of SDH function can be tolerated, and why only in a highly restricted number of cell types. Although loss of function mutations in SDHB-D subunits is almost entirely restricted to oncogenesis, the first description of a loss of function mutation in SDHA was described in neurodegenerative disease, causing Leigh syndrome.[1,5,6] Importantly, the mutations observed in Leigh syndrome are distinct from those reported in tumors, suggesting that mutations in different members of the complex, and indeed different regions of SDHA may have distinct effects on the overall biochemistry of SDH. Indeed, using a model of SDH loss based on deletion of *Sdhb* in a kidney epithelial cell line, it was recently shown that tumor-specific mutations of SDH can compromise activity of complex I,[7,8] while those observed in Leigh syndrome do not.[8] However, data from SDH-deficient PPGL and a chromaffin cell-based model with reduced (knocked-down) Sdhb expression reported around the same time suggested that it may not be the case in this model.[9] The existence of models of SDH deficiency using different cell types therefore provides an opportunity to resolve the question regarding the tissue specificity of tumorigenesis arising from loss of this metabolic enzyme.

It is clear from recent studies in multiple cell models of SDH deficiency that aspects of the TCA cycle retain function.[7,8,10] There is therefore considerable plasticity within the mitochondrial metabolic network, although it is likely that this comes at a cost to the cell—a well-described consequence being the increased production of reactive oxygen species (ROS). These molecules are produced as a result of the dependence of mitochondrial metabolism on redox active reactions. Mitochondrial respiration is based on molecular oxygen accepting electrons that arise from two reduced pyridine nucleotides; NADH and $FADH_2$, which are themselves most often generated through dehydrogenase reactions within the TCA cycle. Loss or reduction of the ability to oxidize these pyridines, as observed in conditions such as hypoxia as well as loss of SDH function, restricts the capability of the TCA cycle to generate the necessary substrates for macromolecule synthesis, such as aspartate.[7,10-12]

It therefore remains unclear what the cellular or microenvironmental conditions are that permit the continued viability and proliferation required for tumorigenesis despite loss of SDH function. We report here that in contrast to epithelial cell models of SDH loss, chromaffin cells lacking SDH retain complex I function, and are capable of oxidizing diverse substrates that may contribute to the metabolic fitness of the cells. However, this comes at a cost to the cell, as they demonstrate little spare respiratory capacity and are highly sensitive to mitochondrial uncoupling. We therefore suggest that at least part of the reason for the restriction of SDH mutation-driven tumors to specific cell types may be due to the retention of complex I activity, reducing the need to remodel the metabolic network associated with the $NADH:NAD^+$ redox pair, allowing continued viability and proliferation.

2 | MATERIALS AND METHODS

2.1 | Cell culture and chemicals

Previously characterized immortalized mouse chromaffin cell lines deficient in *Sdhb* (*Sdhb*$^{-/-}$ CL6 and CL8) as well

as their $Sdhb^{+/+}$ counterparts were maintained in Dulbecco's Modified Eagle Medium (DMEM) supplemented with 10% fetal bovine serum (FBS) and 1 mM pyruvate. The same cell culture conditions were used for the mouse adrenal fibroblasts (MAF), $Sdhb^{+/+}$ and $Sdhb^{-/-}$. All chemicals, including DMEM and FBS, were from Sigma-Aldrich unless stated otherwise. Brightfield images were taken using an EVOS FL (Thermo Scientific), at 10× magnification.

2.2 | High-resolution respirometry

For the measurement in intact state, trypsinized cells were resuspended in cell culture media (4.5 g/L glucose + 1 mM pyruvate) and loaded in an Oxygraph-2k (Oroboros instruments) chamber. After closing the chambers and recording routine respiration, oligomycin (2.5 μM) was added to inhibit ATP synthase. Measurements of the non-phosphorylating electron transfer system (ETS) capacity were obtained through stepwise (0.5 μM) titration of the uncoupler, carbonyl cyanide 4-(trifluoromethoxy)phenylhydrazone (FCCP). Respiration was inhibited by addition of rotenone (0.5 μM) and antimycin A (2.5 μM) at the end of the experiment. For the measurement in permeabilized state, trypsinized and washed cells were resuspended in respiratory media Mir05 (110 mM sucrose, 60 mM K^+-lactobionate, 0.5 mM EGTA, 3 mM $MgCl_2$, 20 mM taurine, 10 mM KH_2PO_4, 20 mM HEPES, 1 g/L BSA [essentially fatty acid free], pH 7.1). After closing the chambers and recording respiration on endogenous substrates, digitonin was added to permeabilize the cells. Substrate combinations were used as indicated in the graphs. The concentrations used were 2 mM malate (Mal), 10 mM glutamate (Glu), 5 mM pyruvate (Pyr), and 10 mM succinate (suc). For fatty acid oxidation (FAO) assessment, limiting malate was used at concentration 0.05 mM and either 40 μM palmitoylcarnitine or 200 μM octanoylcarnitine. In all experiments on permeabilized cells, 3 mM ADP was used and maximum respiratory capacity was reached by stepwise titration of FCCP. Respiration was inhibited by addition of 0.5 μM rotenone and antimycin A (2.5 μM) in the end of the experiment. Values after antimycin A addition were subtracted from all recorded values. For the experiments with ^{13}C tracers, FCCP and inhibitors were omitted. For mitochondrial measurements, the permeabilization step was omitted.

2.3 | Mitochondrial membrane potential measurement

Trypsinized cells were resuspended in Mir05 medium at 0.5 mg/mL protein concentration on ice, and supplemented with 20 nM Tetramethylrhodamine ethyl ester dye (TMRE; Santa Cruz) and respiratory substrates as indicated at concentrations as for the respirometry measurements, before being permeabilized with 0.1 μg digitonin per μg protein for 5 minutes at room temperature and immediately measured on Fortessa LSR-II flow cytometer (Beckton Dickinson). Each set of samples was assessed in three states: untreated (just TMRE and respiratory substrates), state 3 (+3 mM ADP), and uncoupled (100 μM FCCP). The relative mitochondrial membrane potential was determined from the difference of the coupled phosphorylating condition with ADP and the depolarized value.

2.4 | Mitochondrial mass evaluation

Cells in culture were incubated for 20 minutes with 100 nM MitoTracker Green (Thermo Fisher Scientific), before trypsinization, washing (PBS), and resuspension in PBS supplemented with MitoTracker Green (100 nM). Where shown, cells were pre-incubated with FCCP (100 μM) to depolarize the mitochondria 5 minutes before being incubated with MitoTracker Green. The fluorescence signal was assessed using Fortessa LSR-II flow cytometer (Beckton Dickinson), and mitochondrial mass expressed relative to fluorescence signal in $Sdhb^{+/+}$ cells.

For citrate synthase activity, 1×10^6 trypsinized cells were washed with PBS and frozen before lysis in 200 μL of 50 mM Tris (pH 8) with 4 × freeze-thaw cycles in liquid nitrogen/water bath. The assay was performed on 5 μL of cleared supernatant added to 90 μL of reaction buffer (0.1 mM DTNB, 0.3 mM Acetyl CoA, 0.1% Triton X-100 in 100 mM Tris-HCl, pH 8) in 96-well plate. The baseline absorbance was measured in Fluostar Omega plate reader (BMG Labtech) at 412 nm for 15 minutes, then 5 μL of 10 mM oxaloacetate was added and the absorbance measured for further 15 minutes. Baseline signal was subtracted from the signal measured after oxaloacetate addition.

2.5 | ATP assessment

Measurement of cellular ATP was performed using a bioluminescent assay (Sigma; FLAA) as per manufacturer's instructions. 24 hours before measurement, cells were seeded at 2×10^3 per well in a 96-well plate. Where shown, oligomycin (2.5 μM) was added 10 minutes prior to lysis. After removal of media, cells were washed in PBS (pH 7.4) and lysed in 50 μL of buffer. 100 μL of ATP assay was added to all wells before luminescence was read (BMG PHERAstar). Data were normalized to total protein per well using a BCA assay (ThermoFisher Scientific).

2.6 | Total cell protein and cell size evaluation

1×10^6 trypsinized cells were washed with PBS and lysed in 60 μL of RIPA buffer for 30 minutes. Protein concentration in the cleared supernatant was determined using the BCA protein method (Thermo Fisher Scientific). For cell size evaluation, cells were measured in the CASY TT cell counter and their diameter was recorded.

2.7 | Immunoblotting

Cells were lysed in modified RIPA buffer before dilution and quantitation using a bicinchoninic acid (BCA) assay. Lysates were diluted in Laemmli buffer before using 25 μg for electrophoretic separation using SDS-PAGE. After blotting onto nitrocellulose membrane, the following antibodies were used to identify expression of cellular proteins: ACTB, OGDH (Proteintech; #15212-1-AP), PDH E1α (Proteintech; 18068-1-AP), PDHK1 (Cell Signaling; #3820), PDK4 (Proteintech; 12949-1-AP), and PGC1α (Cell Signaling #3820). Images were digitally acquired using a ChemiDoc XRS+ System (Bio Rad).

2.8 | Cell growth assay

Cell growth was assayed using the Sulforhodamine-B (SRB) assay. Cells were plated day before the treatment and after 3 days growth in the presence of the drug cells were fixed in the plates by addition of 20% ice cold trichloracetic acid (TCA) for at least 30 minutes. Fixed cells were then washed with water, left to dry and stained with 0.4% SRB dye dissolved in 1% acetic acid. Superfluous dye was washed off with 1% acetic acid and when dry, dissolved in 50 mM Tris-HCl pH 8 and the absorbance measured on Fluostar Omega plate reader (BMG Labtech) at 510 nm.

2.9 | Mitochondria isolation

Mitochondria were isolated using modified methodology described by Frezza et al.[13] Briefly, trypsinized and washed cells were homogenized for 5 minutes in isolation buffer (200 mM sucrose, 10 mM Tris-MOPS, 1 mM EGTA-Tris; pH 7) using glass/Teflon homogenizer at speed 1000 rpm. Homogenate was then centrifuged at 600 *g* for 10 minutes, pellet discarded, and supernatant centrifuged at 3000 *g* for 5 minutes. Mitochondria in the supernatant were then pelleted at 10 000 *g* for 15 minutes. Pelleted mitochondria were resuspended in ~50 μL of isolation buffer and let stand on ice for at least 1 hour before their respiration was assessed. During this time, protein concentration was determined by BCA protein method (Thermo Fisher Scientific).

2.10 | ^{13}C labeling

Cells were prepared as described for the respirometry measurements and after plasma membrane permeabilization with digitonin, 3 mM ADP and ^{13}C labeled (all CK isotopes) and unlabeled respiratory substrates were added as indicated (1 mM malate, 10 mM glutamate, 5 mM pyruvate, and 3 mM glutamine) and left to respire in opened Oxygraph-2k chambers for 40 minutes. Then the chambers were closed again, respiration signal recorded and cytochrome c was added to check for mitochondrial integrity. Contents of the chambers were collected in precooled Eppendorf tubes, centrifuged at 10 000 *g* for 5 minutes, washed once with ice-cold saline, and frozen immediately on dry ice. For cell-based ^{13}C labeling, $^{13}C_{16}$-palmitic acid (50 μM) or $^{13}C_5$ glutamine (2 mM; all CK Isotopes) were added to cells for 3 days in "flux media"; DMEM powder (Sigma) supplied with sodium bicarbonate as per manufacturer's instructions, 10% FBS and unlabeled forms of glucose and/or glutamine depending on the ^{13}C-enriched nutrient employed. After the incubation period, cells were washed with saline and scraped off the precooled plates into methanol/H_2O mixture. For spent media analysis, 200 μL of cleared media was extracted. In all cases, 0.5 μg/sample of D-6 glutaric acid (CDN Isotopes) supplied in H_2O was used as internal standard and polar metabolites were extracted using Methanol:H_2O:Chloroform at ratio 1:1:1. Briefly, samples were vortexed vigorously, left to shake with all the solvents for 15 minutes at 4°C and then centrifuged for 15 minutes at 16 000 *g*. The upper polar phase was collected and evaporated in the Savant vacuum system (Thermo Fisher Scientific) and used for Gas Chromatography—Mass Spectrometry (GC-MS) analysis.

2.11 | GC-MS analysis

The dried extract was first incubated at 95°C in open tubes and then solubilized in 40 μL of 2% methoxyamine HCl in pyridine followed by 60 minutes incubation at 60°C and subsequently 60 μL N-tertbutyldimethylsilyl-N-methyltrifluoroacetamide with 1% (w/v) tertbutyldimethyl-chlorosilane derivatization reagent was added. The suspension was incubated for an hour at 60°C in a well-sealed tube to prevent evaporation. Finally, the samples were centrifuged at 16 000 *g* for 5 minutes and the clear supernatant was transferred to a chromatography vial with a glass insert (Thermo Fisher Scientific) and processed immediately to GC-MS analysis. For analysis of the derivatized samples, an Agilent 7890B Series GC/MSD gas chromatograph with a polydimethylsiloxane GC column coupled,

with a mass spectrometer (GC-MS) (Agilent Technologies UK Limited, Stockport, UK) was used. Prior to sample analysis, the GC-MS was tuned to a full width at half maximum (FWHM) peak width of 0.60 a.m.u. in the mass range of 50-650 mass to charge ratio (m/z) using PFTBA tuning solution. 1 μL of sample was injected into the GC-MS in splitless mode with helium carrier gas at a rate of 1.0 mL min^{-1}. The inlet liner containing glass wool was set to a temperature of 270°C. Oven temperature was set at 100°C for 1 minute before ramping to 280°C at a rate of 5°C min^{-1}. Temperature was further ramped to 320°C at a rate of 10°C min^{-1} held at 320°C for 5 minutes. Compound detection was carried out in full scan mode in the mass range 50-650 m/z, with 2-4 scans sec^{-1}, a source temperature of 250°C, a transfer line temperature of 280°C and a solvent delay time of 6.5 minutes. The injector needle was cleaned with acetonitrile three times before measurement commencement and three times following every measurement thereafter. The raw GC-MS data were converted to common data format using the acquisition software and further processing of the isotope data including isotope correction and mass isotopomer analysis/batch quantification was performed on metabolite detector software. The raw peak area for each analyte of interest was calculated using the metabolite detector software followed by normalizing the response to the internal standard peak area.

2.12 | Gene expression data

Gene expression profiles of human tumors were available from a previous study, in which 186 fully genotyped PPGL were analyzed.[14,15] The data are shown for a subset of these samples carrying germline and somatic mutations in RET (n = 19), NF1 (n = 37), VHL (n = 40) or SDHx (n = 23) genes, as well as two samples of normal adrenal medulla. HG-U133 Plus 2.0 Affymetrix GeneChip data from this previous study are available online as ArrayExpress entry E-MTAB-733 (http://www.ebi.ac.uk/arrayexpress/). Gene expression profiles of wild-type and *Sdhb*$^{-/-}$ MAF and imCC (CL6 and CL8) were assessed in duplicates using the GeneChip® Mouse Gene 1.0 ST Array.[10] Data are available as ArrayExpress entry E-MTAB-3403. Principal component analysis (PCA) and hierarchical clustering were performed using ClustVis software[16] with default settings using a gene list of 35 PGC1a target genes and metabolic enzymes. Heatmap shows data filtered for genes showing a >1.5-fold difference between WT and KO imCC.

2.13 | Statistical analysis

One-way or two-way ANOVA was used to assess statistical significance; $*P \leq .05$, $**P \leq .01$, $***P \leq .001$, $****P \leq .0001$.

3 | RESULTS

Tumor-associated mutations in SDH, all of which result in loss of oxidative enzymatic activity, lead to tumor formation in a restricted set of cell types—most often chromaffin cells and paraganglia. Previous studies performed in epithelial cell types suggested that mutations in SDH subunits that underpin tumor formation lead to loss of complex I activity and a restricted metabolic phenotype.[8,17] We therefore sought to confirm whether this metabolic phenotype was also observed in a physiologically relevant model derived from chromaffin cells compared to a genetically identical model derived from a non-tumor-forming cell type, adrenal fibroblasts (MAFs).[10] We first assessed oxygen consumption of intact cells and found that although loss of SDH activity in the MAF model decreased oxygen consumption consistent with that previously reported (Figure 1A), SDH-deficient chromaffin cells (imCC) retained a similar respiratory phenotype to their wild-type counterparts (Figure 1B). Interestingly, in both cell models, loss of SDH resulted in no change in ATP synthesis-independent respiration (Figure 1A,B). However, maximal capacity of the electron transport chain (FCCP-uncoupled respiration) was greatly reduced in both SDH-mutated cell models (Figure 1A,B), suggesting that use of electrons in ATP synthesis was reduced independently of cell type. We therefore assessed cellular ATP content between wild-type and SDH-deficient cells, and found that indeed it was significantly lower in both SDH-deficient cell models. To test reliance of the cells on the mitochondrial ATP synthase, we incubated them with the inhibitor, oligomycin, and observed that the wild-type cells were able to compensate with increased glycolytic ATP production, resulting in no net change in cellular ATP (Figure 1C). Interestingly, although the SDH-deficient MAFs also showed a similar ATP content after oligomycin, the SDH-deficient imCC cells demonstrated a significant increase in ATP (Figure 1C). These data demonstrate that the ATP synthase is instead working in reverse in this cell model, hydrolyzing ATP to contribute to the maintenance of the transmembrane proton gradient, much like previously observed in ischemia.[18,19]

To assess mitochondrial respiratory phenotype independently of the cytosol, permeabilized cells were incubated with saturating concentrations of respiratory substrates for complex I, and subsequently complex II. ADP-stimulated (state 3) complex I-supported respiration was found to be lower in the SDH-deficient MAF model compared to wild-type controls, again in contrast to the chromaffin cell model (Figure 1D,E). However, in both models, the expected loss of succinate-driven (complex II) activity was observed in SDH-deficient cells. These data suggest that the loss of complex I activity observed in intact SDH-deficient cells may be through an alteration in the generation or availability of NADH for complex I activity, rather than an

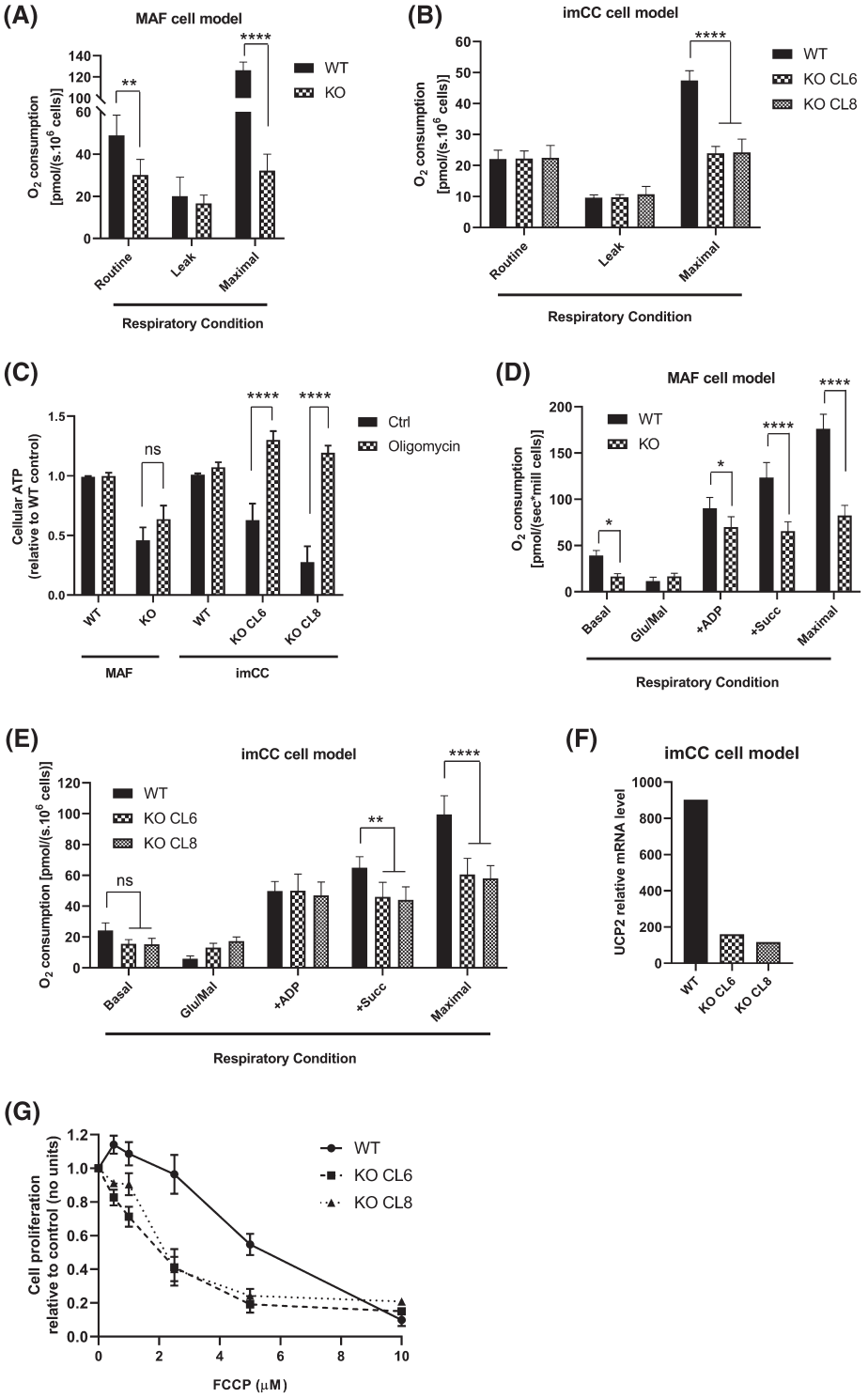

FIGURE 1 A and B, Respiration of intact MAF (A) or imCC (B) cells. Leak was determined through the use of oligomycin (2.5 μM), while maximal condition was defined through addition of FCCP in 0.5 μM steps until maximal rate was observed. Results shown are from 4 (MAF) or 3 (imCC) independent experiments, presented as mean ± SD. Two-way ANOVA was used to assess statistical significance; $^{**}P < .01$, $P < .001$, $^{****}P < .0001$. C, ATP content in both imCC and MAF cell lines, in the presence or absence of oligomycin (2.5 μM, pre-incubated for 10 minutes before lysis), presented as a mean of at least four independent experiments, each in technical triplicate ± SEM. Ns; not significant, $^{****}P < .0001$. D and E, Respiration (oxygen consumption) of permeabilized MAF (D) and imCC (E) cells in basal (Mir05) medium. Additions as follows: Glu/Mal; glutamate (10 mM) and malate (2 mM), ADP (3 mM), Succ; succinate (10 mM) or maximal; FCCP titrated in 0.5 μM steps. Results shown are from four independent experiments, presented as mean ± SD. ns; not significant, $^{*}P < .05$, $^{**}P < .01$, $^{****}P < .0001$. F, UCP2 mRNA expression showing that both Sdhb-deficient clones have >80% reduction in UCP2 expression. G, Effect of the proton ionophore FCCP on cell growth over 3 days in culture. Results are from three independent experiments performed in triplicate, presented as mean ± SEM

inherent defect of mitochondria. Consistent with the data from intact cells, loss of maximal respiratory phenotype (FCCP-stimulated) was observed in permeabilized cells (on complex I and II substrates; Figure 1D,E). These data, alongside those suggesting a reversal of the ATP synthase (Figure 1C) suggested that SDH-deficient cells may be sensitive to uncoupling of the respiratory chain. Indeed, expression of the uncoupling protein, UCP2 was significantly reduced in the SDH-deficient cell models, consistent with this hypothesis (Figure 1F and Supplementary Figure 1A). Importantly, when UCP2 levels were compared between SDH-mutated and non-SDH-mutated patient tumor samples, only the former exhibited reduced expression (Supplementary Figure 1B), confirming that this was a phenotype only relevant to SDH-deficient tumors. We therefore incubated both wild-type and SDH-deficient cells with increasing concentrations of FCCP before assessing cell number after 3 days. We observed a significant sensitization of the SDH-deficient cells, with an LD_{50} around 50% lower than that of wild-type cells (Figure 1G).

Despite the clear similarities between the MAF and imCC cell models, a significant difference was observed in complex I activity between models, with imCC cells retaining activity and the MAF cell model demonstrating a significant reduction in function, as previously described (Figure 1A,B,D,E).[8,17] This suggested that this cell type was able to retain a more wild-type like TCA cycle activity in the absence of SDH compared to the MAFs, which could confer at least part of the tissue specificity of SDH mutant tumors. The respiratory phenotype of the imCCs was therefore investigated in more detail. Previous studies have suggested that the cytosolic redox balance is altered in SDH-deficient cells, and that the addition of exogenous pyruvate can support metabolic function.[7] In addition to supporting cytosolic redox, pyruvate has also been shown as a carbon source in the mitochondria of SDH-deficient cells,[7,10] supporting proliferation (Supplementary Figure 2A). We therefore investigated complex I-linked respiration in permeabilized SDH-deficient cells in the presence of exogenous pyruvate and found that although respiration was unchanged, maximal respiratory capacity was increased (Figure 2A). This suggested that pyruvate oxidation within the mitochondria may be limiting in SDH-deficient cells, perhaps due to a significant demand for oxaloacetate through carboxylation to produce aspartate.[7,10] These data suggested that SDH-deficient imCC cells are not deficient in complex I function, due to the fact that the oxidative decarboxylation of pyruvate is used to reduce NAD^+ to NADH. We therefore tested this using an alternative NADH-producing substrate—fatty acids (FA). During the course of mitochondrial β-oxidation, FA are stepwise degraded to acetyl CoA units. Each of these steps produces $FADH_2$ and NADH, which contribute electrons to the respiratory chain via the electron transport flavoprotein (ETF) and complex I. Using either octanoyl- or palmitoyl-carnitine, we found that both FA are efficient respiratory substrates for SDH-deficient cells (Figure 2B,C). Indeed, respiration on palmitoyl-carnitine exceeded that of the wild-type cells. These measurements provide further confirmation of complex I functionality in SDH-deficient cells and suggest that FA could be an energetic fuel in the absence of full SDH function. This is supported by the fact that SDH-deficient cells showed increased susceptibility to the FA oxidation inhibitor etomoxir (Supplementary Figure 2B), although they showed little difference in the incorporation of palmitate-derived ^{13}C-labeled acetyl CoA units into TCA cycle (Supplementary Figure 2C).

Due to the apparent differences in respiratory capacity and sensitivity to uncoupling, we investigated whether permeabilized SDH-deficient cells maintained a high mitochondrial membrane potential in the presence of saturating concentrations of respiratory substrates. This appeared to be the case (Figure 2D), but when normalized to increased mitochondrial content using MitoTracker Green (Figure 2E), no difference was observed (Figure 2F). Importantly, we confirmed that MitoTracker Green staining was unaffected by mitochondrial membrane potential (Supplementary Figure 2D). As mitochondrial content can also be assessed using citrate synthase activity, this was also examined as an independent measurement, but found not to vary between wild-type and SDH-deficient cells (Figure 2G). These results suggested that SDH-deficient cells may upregulate their mitochondrial mass to compensate for reduced metabolic efficiency arising through mechanisms such as ROS-mediated damage of matrix proteins, or reduced matrix protein content—the latter resulting in a less dense matrix. Respiratory experiments performed on isolated mitochondria support this observation, as these show decreased respiration on glutamate/malate combination and similar respiration in the presence of glutamate/malate/pyruvate when expressed per mitochondrial protein (Figure 2H). Importantly, SDH-deficient cells are larger than their wild-type counterparts (Figure 2I and Supplementary Figure 2E,F)—consistent with them containing enlarged mitochondria (Figure 2E). We therefore investigated whether SDH-deficient cells increase PGC1a expression as a marker of increased mitochondrial biogenesis, but found instead decreased expression (Supplementary Figure 2G). These data suggest that the change in mitochondrial mass is unlikely to be due to increased biogenesis, but more likely due to matrix swelling as a result of metabolic dysfunction.

To investigate the metabolic pathways that SDH-deficient cells use to support complex I-linked respiration in more depth, we investigated the metabolism of $^{13}C_4$-malate supplied to permeabilized cells as before (G+M; Figure 3A), but incubated for 45 minutes—a time point previously shown to approach steady state.[20] Although

limited incorporation of ^{13}C from malate was observed in succinate (Figure 3B), which is most likely due to the presence of unlabeled glutamate, we observed similar labeling of m + 4 citrate between wild-type and SDH-deficient cells, indicative of citrate synthase activity. This was confirmed by similar levels of the m + 6 citrate isotopomer, which is the product of the condensation of $^{13}C_4$-oxaloacetate (OAA) and $^{13}C_2$-acetyl CoA (Figure 3C). Labeling of acetyl CoA occurs through oxidation of labeled pyruvate, which itself is derived either from OAA or malate through the action of

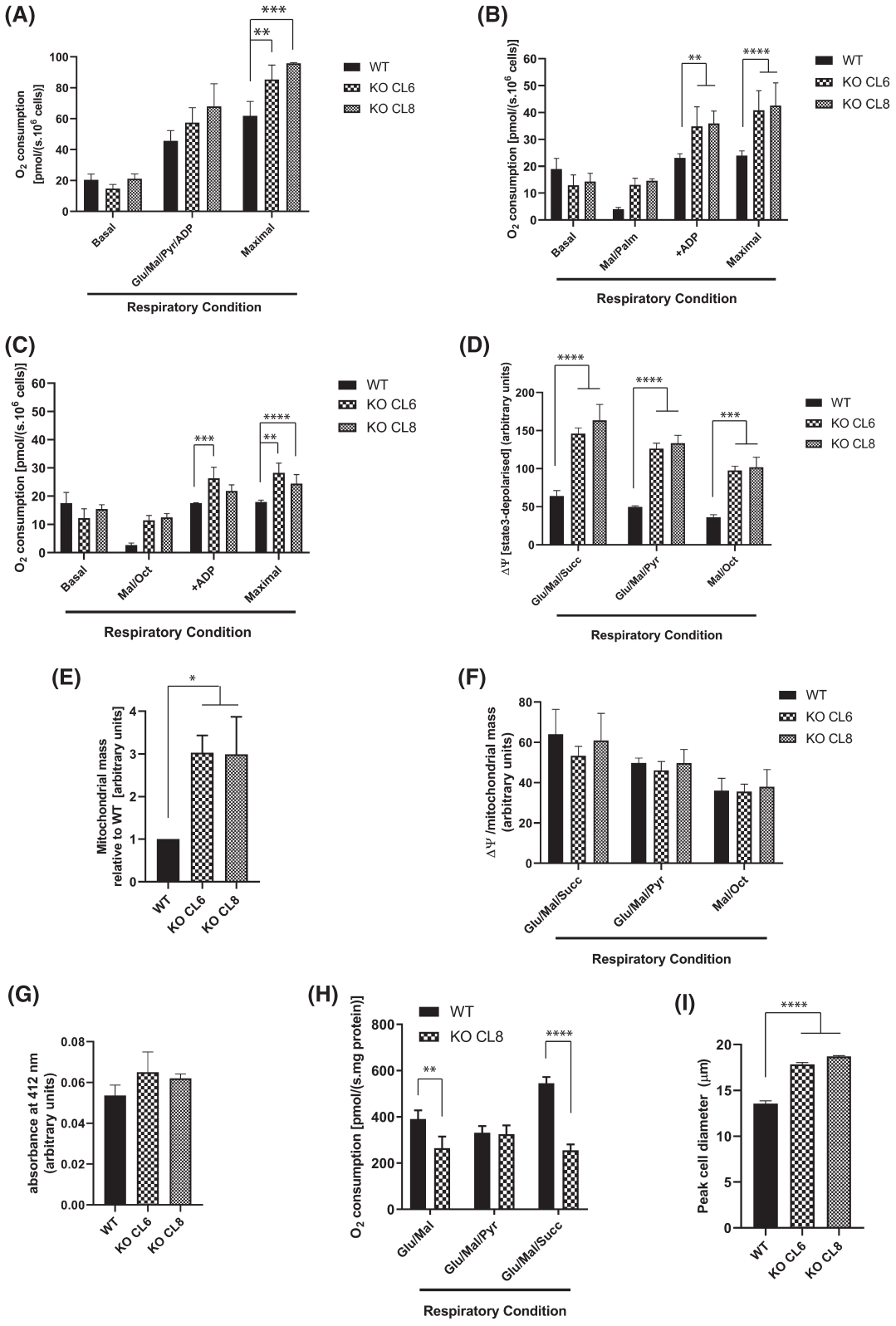

FIGURE 2 A, Respiration (oxygen consumption) of permeabilized imCCs in basal state (Mir05 medium), or with the following additions: Glu/Mal/Pyr/ADP; glutamate (10 mM), malate (2 mM) and pyruvate (5 mM), ADP (3 mM), followed by FCCP to stimulate maximal respiration. *$P < .05$, **$P < .01$ (two-way ANOVA, Dunnett's post-test). B and C, Respiration of fatty acids—palmitate (B) and octanoate (C). Palmitoylcarnitine (40 μM) or octanoylcarnitine (200 μM) were added with limiting concentrations of malate (0.05 mM), with ADP (3 mM), followed by FCCP (maximal) to stimulate maximal respiration as above. **$P < .01$, ***$P < .001$, ****$P < .001$ (two-way ANOVA, Dunnett's post-test). D, Mitochondrial membrane potential ($\Delta\psi$) assessed in the presence of indicated substrates. The substrates were: 10 mM glutamate (Glu), 2 mM malate (Mal), 5 mM pyruvate (Pyr), 10 mM succinate (Succ), or 200 μM octanoylcarnitine and 0.05 M malate (Mal/Oct). ***$P < .001$, ****$P < .001$ (two-way ANOVA, Dunnett's post-test). E, Mitochondrial mass assessed with 100 nM of $\Delta\psi$ insensitive dye MitoTracker Green. $P < .05$ (t test with Welch's correction). F, $\Delta\psi$ normalized to mitochondrial mass ([data shown in D]/[data shown in E]). G, Citrate synthase activity assessed per cell number. H, Respiration of isolated mitochondria in the presence of 3 mM ADP and different substrate combinations as indicated. The substrates were 10 mM glutamate (Glu), 2 mM malate (Mal), 5 mM pyruvate (Pyr), and 10 mM succinate (Succ). **$P < .01$, ****$P < .0001$ (two-way ANOVA, Dunnett's post-test). I, Cell size presented as peak diameter (PDI) of the cells in suspension. ****$P < .0001$. Results shown are from 3 to 4 independent experiments and presented as mean ± SD, apart from G and I, which were 4 and 3 independent samples, respectively

mitochondrial phosphoenolpyruvate carboxykinase (PCK2) or malic enzyme (ME2) activities, respectively (Figure 3A). High levels of pyruvate-forming activity in these conditions were confirmed through the presence of the m + 3 isotopomer of alanine (Figure 3D).[21] We and others have previously shown upregulation of pyruvate carboxylase in SDH-deficient cells and tumors, which would support anaplerotic pyruvate use in the mitochondria.[7,10] In light of the results above, we investigated the expression of enzymes involved in central carbon metabolism in the mitochondria, and observed a number with significant differential changes in mRNA expression between MAF and imCC model (Supplementary Figure 3A). Given that PDHA1 and PDK4, two enzymes involved in the regulation of pyruvate oxidation, demonstrated altered expression, we assessed them at the protein level and found that they were both significantly downregulated, but in both cell models (Supplementary Figure 3B). These data suggest that changes in pyruvate oxidation that may occur downstream of these alterations in protein expression are unlikely to explain cell type-specific metabolic alterations observed.

To investigate TCA cycle pathways downstream of citrate, we omitted glutamate from the system and used either a combination of $^{13}C_4$-malate and unlabeled pyruvate (Figure 3E), or $^{13}C_5$-glutamine/unlabeled malate (Figure 3I). When $^{13}C_4$-malate was supplied together with unlabeled pyruvate, clear evidence of citrate synthase activity in both cell lines was observed (m + 4 isotopomer), which constituted 90% of the total citrate pool in SDH-deficient cells and 70% in wild-type (Figure 3F). Continued oxidation of citrate to yield succinate appeared to be higher in SDH-deficient cells compared to wild-type cells (m + 2 succinate isotopomer; Figure 3G) confirming the absence of any metabolic defect in the TCA cycle between citrate synthase and SDH, and therefore efficient NADH-oxidizing activity in the SDH-deficient chromaffin cells. The mass isotopomer distribution is independent of pool size so this difference is expected to be independent of the truncation of the TCA cycle in SDH-deficient cells and concomitant succinate accumulation. In both cell lines, 90% of all fumarate was synthesized through fumarate hydratase activity, suggestive of relatively low SDH activity even in wild-type chromaffin cells (Figure 3H). When the permeabilized cells were incubated with unlabeled malate in combination with $^{13}C_5$ glutamine, around 80% of all citrate was unlabeled in SDH-deficient cells while this was ~60% in wild-type cells, the predominant isotopomers arose from TCA cycle oxidation activity (m + 2 and m + 4 isotopomers; Figure 3J). Interestingly, although glutamine-derived glutamate was similar in both conditions (Figure 3K), downstream production of succinate was increased in SDH-deficient cells, as expected (Figure 3L). These results suggest that the respiratory substrates provided to mitochondria in selectively permeabilized cells are metabolized in a similar manner independent of SDH function. We have previously shown that expression of many of the enzymes involved in the reductive carboxylation of glutamine is altered independently of cell model at the mRNA level.[10] Due to the increased glutamate oxidation observed, we investigated the expression of 2-oxoglutarate (α-ketoglutarate) dehydrogenase (OGDH), part of the OGDH complex, and a critical control point for glutamate oxidation within TCA cycle. We found that it was not substantially altered in either cell model (Supplementary Figure 3C).

It was recently shown that after pharmacological inhibition of SDH, complex I-dependent respiration was preserved due to glutamine oxidation accompanied by succinate efflux out of mitochondria and the cell.[8] It was further suggested that this mechanism sustains respiration in cells with neurodegeneration-associated *SDHA* mutation and suggested that the ability to use this normally redundant metabolic shunt may explain the different phenotype in SDH-mutations-associated tumors versus neurodegenerative disorders.[8] In our study, we report that respiration was found to be similar between wild-type and SDH-deficient chromaffin cells (Figure 1B) due to a maintenance of complex I activity. We therefore investigated whether succinate efflux specifically supported glutamine oxidation in our model. We incubated SDH-deficient cells with $^{13}C_5$-glutamine, and indeed observed a high rate of glutamine-derived succinate efflux, with close to 75% of all

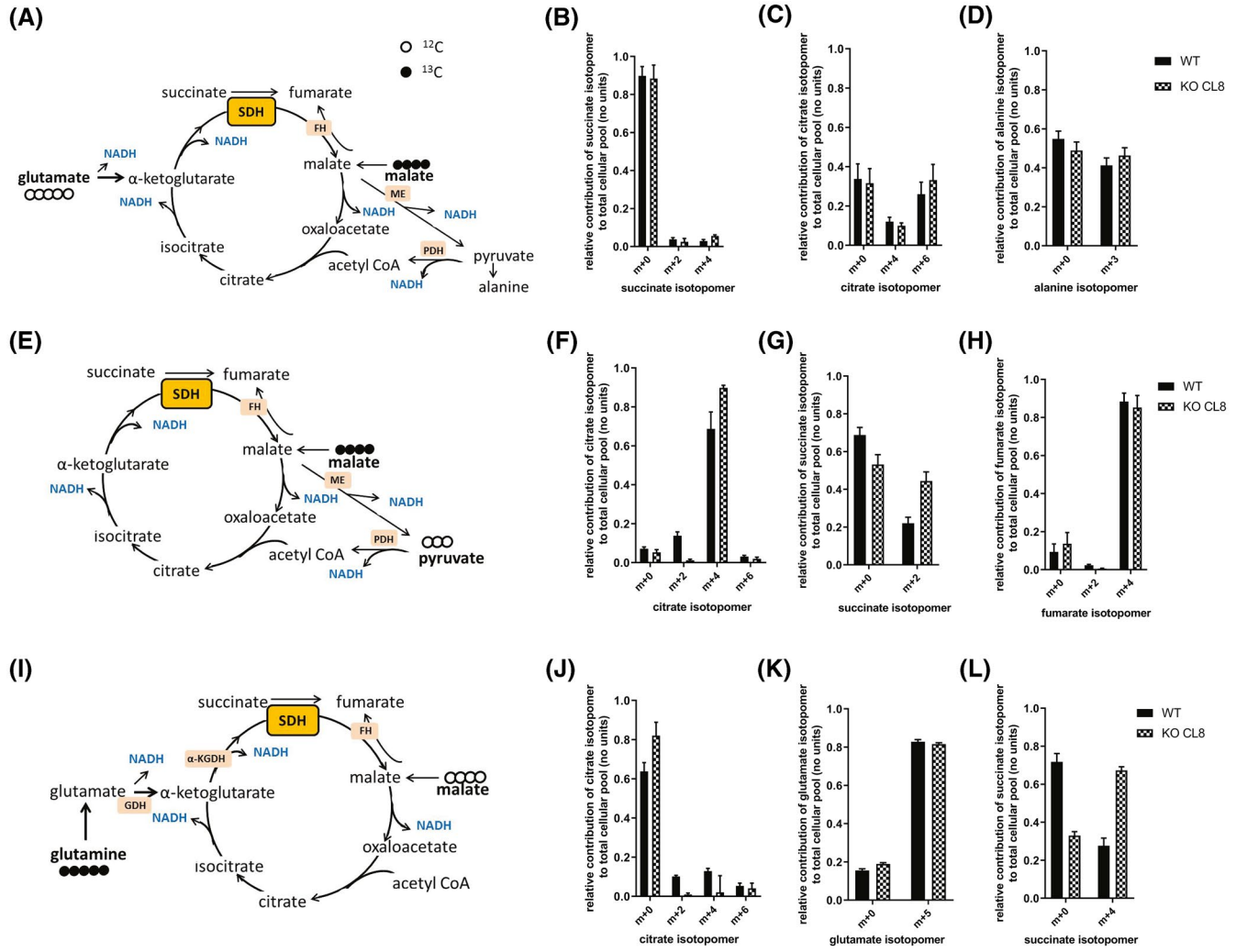

FIGURE 3 Metabolism of ^{13}C labeled respiratory substrates. A, Scheme of TCA cycle with SDH enzyme (yellow box) and accompanying redox reaction producing NADH (highlighted in blue) during the labeling experiment with $^{13}C_4$ malate and non-labeled glutamate in the Oxygraph-2k. Black full circles represent ^{13}C carbon atoms. B-D, Relative contribution of succinate (B), citrate (C), and alanine (D) isotopomers to total cellular pool in the Oxygraph-2k labeling experiment with 1 mM $^{13}C_4$ malate and unlabeled 10 mM glutamate. E, Scheme of TCA cycle with SDH enzyme (yellow box) and accompanying redox reaction producing NADH (highlighted in blue) during the labeling experiment with $^{13}C_4$ malate and non-labeled pyruvate in the Oxygraph-2k. Black full circles represent ^{13}C carbon atoms. F-H, Relative contribution of citrate (F), succinate (G), and fumarate (H) isotopomers to total cellular pool in the Oxygraph-2k labeling experiment with 1 mM $^{13}C_4$ malate and non-labeled 5 mM pyruvate. I, Scheme of TCA cycle with SDH enzyme (yellow box) and accompanying redox reaction producing NADH (highlighted in blue) during the labeling experiment with $^{13}C_5$ glutamine and non-labeled malate in the Oxygraph-2k. Black full circles represent ^{13}C carbon atoms. J-L, Relative contribution of citrate (J), glutamate (K), and succinate (L) isotopomers to total cellular pool in the Oxygraph-2k labeling experiment with 3 mM $^{13}C_5$ glutamine with non-labeled 1 mM malate. Data shown are a product of 2-3 independent experiments performed in duplicate and individual results pooled for final evaluation presented as mean ± SD

cellular succinate arising from glutamine (compared to 32% in wild-type cells; Figure 4A), which was also observed in the medium (Figure 4B,C). This suggests that glutamine oxidation is highly active in the chromaffin model of *Sdhb* loss, and could explain the sustained respiration observed. Consistent with their increased glutamine requirement, inhibition of glutaminolysis with BPTES, a potent inhibitor of glutaminase, reduced growth or increased cell death of SDH-deficient cells more efficiently than in their wild-type counterparts (Figure 4D).

4 | DISCUSSION

SDH-mutated tumors arise from one of very few cell types, which include chromaffin cells, paraganglia, and gastrointestinal stromal cells.[22] Given that these cell types have not been shown to have a higher inherent rate of mutation than others, it suggests that they are able to tolerate loss of this central metabolic enzyme while other cell types cannot. Indeed, this is a common theme in tumors driven by mutations in metabolic enzymes: loss of fumarate hydratase

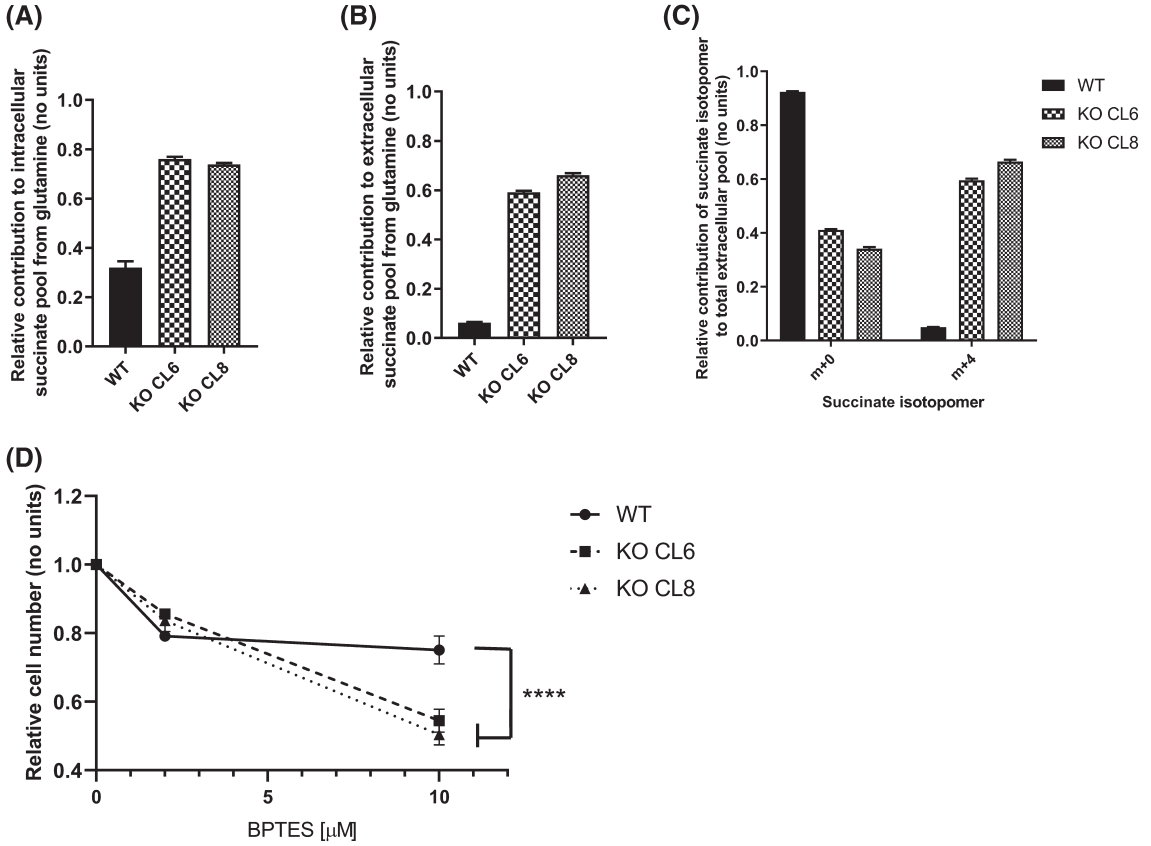

FIGURE 4 Glutamine oxidation and succinate efflux in *Sdhb*$^{-/-}$ cells. A, Relative contribution to intracellular succinate pool from $^{13}C_5$ glutamine. B, Relative contribution to effluxed succinate pool from $^{13}C_5$ glutamine. C, Relative contribution of succinate isotopomers to total extracellular succinate pool from $^{13}C_5$ glutamine. D, Cell growth over period of 3 days in the presence of 2 or 10 μM BPTES. In (A-C), experiments were done in tetraplicate and results shown are presented as mean ± SD. In (D) 4, independent experiments were done in triplicate and results are shown as mean ± SEM. One-way ANOVA was used to assess statistical significance; ****$P \leq .0001$

is observed to arise most frequently in myocytes of the smooth muscle and renal epithelium while oncogenic mutations in isocitrate dehydrogenase 1 are most often observed in tumors arising from glial cells, myeloid cells, and chondrocytes.[22]

This study represents the first to investigate comprehensively mitochondrial metabolic function after loss of *Sdhb*, in chromaffin cells. It is important to note that many of the metabolic phenotypes observed in the chromaffin model described here and published previously mirror those described in other *Sdhb*$^{-/-}$ models based on non-physiologically relevant cell types; adrenal fibroblast (described here), renal,[7,8] and breast epithelia.[17] In these models, both respiration of intact cells and complex I-specific activity were found to be lower in SDH-deficient cells compared with wild-type (Figure 1).[7,8,17] We show here that this is not the case in a chromaffin cell-derived model, which retains complex I function and a respiratory activity comparable to wild-type cells. Furthermore, it appears that they maintain the supply of acetyl co-A through a combination of pyruvate and fatty acid oxidation. However, our data also suggest that when FA oxidation is inhibited, SDH-deficient chromaffin cells are unable to compensate with additional contribution from pyruvate, which is most likely due to inhibition of pyruvate dehydrogenase by HIF-dependent upregulation of the inhibitory kinase, pyruvate dehydrogenase kinase 1 (Supplementary Figure 3B).[23] Finally, we also provide evidence to suggest that in the imCC cell model, the mitochondrial ATP synthase functions as an ATP-hydrolyzing proton pump, in contrast to the MAF cell model. This is consistent with the increased sensitivity of these SDH-deficient cells to the ionophore, FCCP (Figure 1G), which dissipates the proton gradient and therefore likely increases the rate of mitochondrial ATP hydrolysis to a rate that is unsustainable for the cells.

It is important to note that some of the respiratory phenotype observed in the chromaffin model is likely due to the increased mitochondrial mass observed that was not apparent in the breast epithelial model.[17] Increased mitochondrial mass downstream of SDH deficiency is consistent with previous observations made in *SDH*-mutated

PPGL, which are characterized by the presence of significant number of defective mitochondria.[24,25] Indeed, a similar mitochondrial morphology and increase in mass was observed in other SDHB-mutated tumor types as well as in *Sdhb*$^{+/-}$ mice.[26,27] However, this increase may come at a cost to the cell; the mitochondria themselves are less efficient, and even small increases in electron flow were found to result in a reduction in viability (Figure 1G). Importantly, the clear differences between the chromaffin and non-chromaffin cell models observed in this study are also reflected in previous studies using these models, where glucose and glutamine oxidation, which generate NADH, were retained in the *Sdhb*$^{-/-}$ chromaffin cell model, which was less apparent in the epithelial cell models.[7,10]

It is therefore clear from the cell model data both previously published and presented here that, in parallel with the etiology of SDHB-deficient tumors, the tissue of origin of the SDH-deficient cell may be critical to their ability to cope with loss of SDH activity. We suggest that at least some of this is likely due to the retention of complex I function, which maintains a more favorable NAD^+:NADH, reducing the need for additional metabolic re-wiring. The respiration of SDH-deficient cells is supported by increased but incomplete glutamine oxidation. However, this is not sufficient to ensure reserve respiratory capacity and these cells show high sensitivity toward inhibition of glutaminolysis and mitochondrial uncoupling, features which could be taken advantage of for future therapeutic potential.

ACKNOWLEDGMENTS

We would like to thank Professor Mark Viant and Dr Stefan Schade for the use and assistance with the CASY cell counter. We thank Professors Ed Rainger and David Hodson and Mr Nick Fine for kindly providing reagents. KK, AT, and JG are supported by the Paradifference Foundation, LV, CEG, and BK are supported by Cancer Research UK (C42109/A26982 and C42109/A24891) and GGL holds a Wellcome Trust Senior Fellowship (104612/Z/14/Z).

AUTHORS CONTRIBUTIONS

K. Kľučková, C. Escribano-Gonzalez, L. Vettore, R.L. Hindshaw, J.L.E. Tearle, and B. Kaul performed research; J. Goncalves and G.G. Lavery prepared and supplied reagents; K. Kľučková, C. Escribano-Gonzalez, L. Vettore, R.L. Hindshaw, J.L.E. Tearle, A. Thakker, J. Favier, and D.A. Tennant processed and analyzed data; K. Kľučková, J. Favier, and D.A. Tennant designed the research and wrote the manuscript.

CONFLICT OF INTEREST

The authors declare no conflicts of interest.

REFERENCES

1. Bardella C, Pollard PJ, Tomlinson I. SDH mutations in cancer. *Biochim Biophys Acta*. 2011;1807:1432-1443.
2. Letouze E, Martinelli C, Loriot C, et al. SDH mutations establish a hypermethylator phenotype in paraganglioma. *Cancer Cell*. 2013;23:739-752.
3. Selak MA, Armour SM, MacKenzie ED, et al. Succinate links TCA cycle dysfunction to oncogenesis by inhibiting HIF-alpha prolyl hydroxylase. *Cancer Cell*. 2005;7:77-85.
4. Baysal BE, Ferrell RE, Willett-Brozick JE, et al. Mutations in SDHD, a mitochondrial complex II gene, in hereditary paraganglioma. *Science*. 2000;287:848-851.
5. Bourgeron T, Rustin P, Chretien D, et al. Mutation of a nuclear succinate dehydrogenase gene results in mitochondrial respiratory chain deficiency. *Nat Genet*. 1995;11:144-149.
6. Burnichon N, Briere JJ, Libe R, et al. SDHA is a tumor suppressor gene causing paraganglioma. *Hum Mol Genet*. 2010;19:3011-3020.
7. Cardaci S, Zheng L, MacKay G, et al. Pyruvate carboxylation enables growth of SDH-deficient cells by supporting aspartate biosynthesis. *Nat Cell Biol*. 2015;17:1317-1326.
8. Lorendeau D, Rinaldi G, Boon R, et al. Dual loss of succinate dehydrogenase (SDH) and complex I activity is necessary to recapitulate the metabolic phenotype of SDH mutant tumors. *Metab Eng*. 2017;43:187-197.
9. Pang Y, Lu Y, Caisova V, et al. Targeting NAD(+)/PARP DNA Repair Pathway as a Novel Therapeutic Approach to SDHB-Mutated Cluster I Pheochromocytoma and Paraganglioma. *Clin Cancer Res*. 2018;24:3423-3432.
10. Lussey-Lepoutre C, Hollinshead KE, Ludwig C, et al. Loss of succinate dehydrogenase activity results in dependency on pyruvate carboxylation for cellular anabolism. *Nat Commun*. 2015;6:8784.
11. Birsoy K, Wang T, Chen WW, Freinkman E, Abu-Remaileh M, Sabatini DM. An essential role of the mitochondrial electron transport chain in cell proliferation is to enable aspartate synthesis. *Cell*. 2015;162:540-551.
12. Sullivan LB, Gui DY, Hosios AM, Bush LN, Freinkman E, Vander Heiden MG. Supporting aspartate biosynthesis is an essential function of respiration in proliferating cells. *Cell*. 2015;162:552-563.
13. Frezza C, Cipolat S, Scorrano L. Organelle isolation: functional mitochondria from mouse liver, muscle and cultured fibroblasts. *Nat Protoc*. 2007;2:287-295.
14. Ben Aim L, Pigny P, Castro-Vega LJ, et al. Targeted next-generation sequencing detects rare genetic events in pheochromocytoma and paraganglioma. *J Med Genet*. 2019;56:513-520.
15. Burnichon N, Vescovo L, Amar L, et al. Integrative genomic analysis reveals somatic mutations in pheochromocytoma and paraganglioma. *Hum Mol Genet*. 2011;20:3974-3985.
16. Metsalu T, Vilo J. ClustVis: a web tool for visualizing clustering of multivariate data using Principal Component Analysis and heatmap. *Nucleic Acids Res*. 2015;43:W566-W570.
17. Bezawork-Geleta A, Wen H, Dong L, et al. Alternative assembly of respiratory complex II connects energy stress to metabolic checkpoints. *Nat Commun*. 2018;9:2221.
18. Rouslin W. Protonic inhibition of the mitochondrial oligomycin-sensitive adenosine 5′-triphosphatase in ischemic and autolyzing cardiac muscle. Possible mechanism for the mitigation of ATP hydrolysis under nonenergizing conditions. *J Biol Chem*. 1983;258:9657-9661.

19. Garlick PB, Radda GK, Seeley PJ. Studies of acidosis in the ischaemic heart by phosphorus nuclear magnetic resonance. *Biochem J*. 1979;184:547-554.
20. Nonnenmacher Y, Palorini R, d'Herouel AF, et al. Analysis of mitochondrial metabolism in situ: Combining stable isotope labeling with selective permeabilization. *Metab Eng*. 2017;43:147-155.
21. Christen S, Lorendeau D, Schmieder R, et al. Breast cancer-derived lung metastases show increased pyruvate carboxylase-dependent anaplerosis. *Cell Rep*. 2016;17:837-848.
22. Laurenti G, Tennant DA. Isocitrate dehydrogenase (IDH), succinate dehydrogenase (SDH), fumarate hydratase (FH): three players for one phenotype in cancer? *Biochem Soc Trans*. 2016;44:1111-1116.
23. Kim JW, Tchernyshyov I, Semenza GL, Dang CV. HIF-1-mediated expression of pyruvate dehydrogenase kinase: a metabolic switch required for cellular adaptation to hypoxia. *Cell Metab*. 2006;3:177-185.
24. Douwes Dekker PB, Hogendoorn PC, Kuipers-Dijkshoorn N, et al. SDHD mutations in head and neck paragangliomas result in destabilization of complex II in the mitochondrial respiratory chain with loss of enzymatic activity and abnormal mitochondrial morphology. *J Pathol*. 2003;201:480-486.
25. D'Antongiovanni V, Martinelli S, Richter S, et al. The microenvironment induces collective migration in SDHB-silenced mouse pheochromocytoma spheroids. *Endocr Relat Cancer*. 2017;24:555-564.
26. Housley SL, Lindsay RS, Young B, et al. Renal carcinoma with giant mitochondria associated with germ-line mutation and somatic loss of the succinate dehydrogenase B gene. *Histopathology*. 2010;56:405-408.
27. Szarek E, Ball ER, Imperiale A, et al. Carney triad, SDH-deficient tumors, and Sdhb+/- mice share abnormal mitochondria. *Endocr Relat Cancer*. 2015;22:345-352.

SUPPORTING INFORMATION

Additional supporting information may be found online in the Supporting Information section.

How to cite this article: Kľučková K, Thakker A, Vettore L, et al. Succinate dehydrogenase deficiency in a chromaffin cell model retains metabolic fitness through the maintenance of mitochondrial NADH oxidoreductase function. *The FASEB Journal*. 2020;34:303–315. https://doi.org/10.1096/fj.201901456R